ENKD1 promotes CP110 removal through competing with CEP97 to initiate ciliogenesis

Ting Song[1,†] ![ID], Yunfan Yang[2,†] ![ID], Peng Zhou[1], Jie Ran[1] ![ID], Liang Zhang[1], Xiaofan Wu[3], Wei Xie[1] ![ID], Tao Zhong[1] ![ID], Hongbin Liu[2] ![ID], Min Liu[1], Dengwen Li[3], Huijie Zhao[1,*] ![ID] & Jun Zhou[1,3,**] ![ID]

Abstract

Despite the importance of cilia in cell signaling and motility, the molecular mechanisms regulating cilium formation remain incompletely understood. Herein, we characterize enkurin domain-containing protein 1 (ENKD1) as a novel centrosomal protein that mediates the removal of centriolar coiled–coil protein 110 (CP110) from the mother centriole to promote ciliogenesis. We show that *Enkd1* knockout mice possess ciliogenesis defects in multiple organs. Super-resolution microscopy reveals that ENKD1 is a stable component of the centrosome throughout the ciliogenesis process. Simultaneous knockdown of ENKD1 and CP110 significantly reverses the ciliogenesis defects induced by ENKD1 depletion. Protein interaction analysis shows that ENKD1 competes with centrosomal protein 97 (CEP97) in binding to CP110. Depletion of ENKD1 enhances the CP110–CEP97 interaction and detains CP110 at the mother centriole. These findings thus identify ENKD1 as a centrosomal protein and uncover a novel mechanism controlling CP110 removal from the mother centriole for the initiation of ciliogenesis.

Introduction

Cilia are highly conserved microtubule-based organelles that protrude from the surface of most mammalian cells. Cilia are traditionally classified into two groups, primary cilia and motile cilia. Primary cilia are typically immotile and play important roles in sensing and transducing environmental cues (Anvarian *et al*, 2019; Nachury & Mick, 2019), whereas motile cilia are able to generate fluid flow in tissues such as the airway and brain ventricle epithelium (Spassky & Meunier, 2017; Liu *et al*, 2020; Pellicciotta *et al*, 2020). Defects in the structures and/or functions of cilia are associated with a variety of human diseases, collectively called ciliopathies (Yang *et al*, 2014; Reiter & Leroux, 2017). For example, primary cilia are present in the retina of the eye, and their abnormal assembly or functional impairment can cause retinal degeneration (Buskin *et al*, 2018; Mookherjee *et al*, 2018). Another example is the presence of motile cilia in the airway epithelium, and the abnormal assembly is a major cause of recurrent respiratory infections and impaired mucociliary clearance (Chivukula *et al*, 2020; Wallmeier *et al*, 2020).

Ciliogenesis is a multi-step process that typically involves the formation of the basal body, assembly of the transition zone, and extension of the axoneme (Tu *et al*, 2018; Walia *et al*, 2019). Centrosomes are major microtubule-organizing centers in mammalian cells (Paz & Lüders, 2018; Meitinger *et al*, 2020). At the core of the centrosome are two cylindrical structures termed as mother centriole and daughter centriole. The mother centriole can be distinguished by its distal and subdistal appendages (Mönnich *et al*, 2018). Certain centrosomal proteins, such as centrosomal protein 192 (CEP192), CEP135, polo-like kinase 4 (PLK4), and centrosomal P4.1-associated protein (CPAP), have been identified as indispensable components for the assembly of centrosome structures (Carvalho-Santos *et al*, 2010; Nigg & Holland, 2018). During ciliogenesis, the mother centriole transforms into the basal body. Ciliary membrane establishment requires components of the Rab-GTPase cascade, such as Rab11 and Rab8, for the intracellular membrane trafficking (Knödler *et al*, 2010; Walia *et al*, 2019), and CEP164 for ciliary vesicle docking at the mother centriole (Schmidt *et al*, 2012; Čajánek & Nigg, 2014). Transition zone proteins are recruited to the mother centriole as the ciliary vesicle develops into the ciliary sheath membrane, which also tightly coincides with the growth of the axonemal microtubule doublet (Williams *et al*, 2011; Vieillard *et al*, 2016).

Negative regulators of cilium assembly, in particular, the CP110-CEP97 protein complex, need to be removed from the mother centriole to initiate ciliogenesis (Spektor *et al*, 2007). CP110 localizes to

1 Shandong Provincial Key Laboratory of Animal Resistance Biology, Institute of Biomedical Sciences, College of Life Sciences, Collaborative Innovation Center of Cell Biology in Universities of Shandong, Shandong Normal University, Jinan, China
2 Cheeloo College of Medicine, Shandong University, Jinan, China
3 State Key Laboratory of Medicinal Chemical Biology, Haihe Laboratory of Cell Ecology, Department of Genetics and Cell Biology, College of Life Sciences, Nankai University, Tianjin, China
*Corresponding author. Tel: +86 531 8618 2518; E-mail: huijiezhao@sdnu.edu.cn
**Corresponding author. Tel: +86 531 8618 2518; E-mail: junzhou@sdnu.edu.cn
†These authors contributed equally to this work

the distal end of centrioles (Chen *et al*, 2002), and regulates centriole length by preventing centriolar microtubule extension (Kleylein-Sohn *et al*, 2007; Schmidt *et al*, 2009; Shoda *et al*, 2021). However, CP110 does not regulate cilium length, indicating that cilium elongation is a further step (Spektor *et al*, 2007). CEP97 is a conserved protein that also regulates centriole elongation, and might serve as a chaperone to stabilize CP110, allowing the co-recruitment of both proteins to the centrosome (Bettencourt-Dias & Carvalho-Santos, 2008; Dobbelaere *et al*, 2020). Removal of CP110 is critical for the conversion of the mother centriole to the basal body, and the presence of CP110 has been found to hinder cilium formation (Cao *et al*, 2012). However, the precise molecular mechanisms orchestrating CP110 removal remain elusive. In this study, our data demonstrate that ENKD1 is a component of the centrosome and promotes ciliogenesis by stimulating the removal of the CP110–CEP97 protein complex from the mother centriole.

Results

Enkd1 knockout mice display ciliogenesis defects in multiple organs

In a mass spectrometry-based effort to uncover novel regulators of ciliogenesis, we identified ENKD1 in the centrosomal fractions of RPE1 human retinal pigment epithelial cells. In order to study the function of this protein, we generated *Enkd1* knockout mice by using the CRISPR/Cas9 technology. The depletion of ENKD1 in the knockout mice was confirmed at both genomic and protein levels (Fig 1A–C). We then performed immunoblot analysis to examine the expression of ENKD1 in mouse tissues, and found that ENKD1 proteins were present in multiple tissues and overexpressed in the testis and lung (Fig EV1A), suggesting a universal expression of ENKD1 in tissues. Unexpectedly, *Enkd1* knockout mice were born at the expected Mendelian ratio. Young adult *Enkd1* knockout mice (6–12 weeks old) showed no gross defects in growth or survival when they were housed in a pathogen-free condition.

To determine the potential role of ENKD1 in ciliogenesis, we first analyzed cilia in the mouse retina by immunostaining of acetylated α-tubulin, a well-known ciliary marker (L'Hernault & Rosenbaum, 1985). We found that the number of retinal photoreceptor cilia was greatly decreased in *Enkd1* knockout mice, but the length of existing cilia was not significantly affected, as compared to wild-type mice (Fig 1D–F). Next, we measured the electroretinogram (ERG) and the flash visual evoked potential (F-VEP) to evaluate the effects of ENKD1 depletion on functional integrity of the retina (Ridder & Nusinowitz, 2006). *In vivo* ERG analysis of light response was recorded from dark-adapted mice. Strikingly, significant reductions in the amplitude of the ERG a- and b-wave were observed in *Enkd1* knockout mice (Fig 1G and H). The F-VEP components of the *Enkd1* knockout mice also displayed a significantly reduced voltage amplitude compared to those of wild-type mice (Fig 1I and J). These data indicate a defective vision of *Enkd1* knockout mice. Moreover, we examined primary cilia in kidneys from wild-type mice and *Enkd1* knockout mice. A decrease in the number of renal cilia, but not the average ciliary length, was also observed in *Enkd1* knockout mice, as compared to wild-type mice (Fig 1K–M).

Since primary cilia play essential roles in heart development (Willaredt *et al*, 2012; Klena *et al*, 2017; Pala *et al*, 2018), surface electrocardiography (ECG) was utilized to evaluate the cardiac function. We observed that the average R-wave duration of *Enkd1* knockout mice was significantly reduced compared with that of wild-type mice, and the QRS duration displayed a modest reduction as well (Fig EV1B–F). Furthermore, the RR interval (the time elapsed between two successive R waves) was prolonged, although the difference did not reach statistical significance (Fig EV1C and G). Thus, these data indicate that the conduction system of the heart is moderately altered due to the loss of ENKD1.

Although the *Enkd1* knockout males were normally fertile, a significant increase in the number of aberrant spermatozoa with no tails was observed (Fig 1N and O). However, the flagellated sperm in *Enkd1* knockout mice maintained normal flagellar length and displayed normal motility (Fig 1N, P and Q), consistent with the

---

Figure 1. *Enkd1* knockout mice display ciliogenesis defects in multiple organs.

A   Strategy for the generation of *Enkd1* knockout mice. Deletion of a fragment containing the 173 bp exon 3 and adjacent flanking sequences results in the disruption of ENKD1 protein expression.
B   Identification of wild-type (WT), heterozygous (HZ), and knockout (KO) mice by PCR and agarose gel electrophoresis.
C   Immunoblotting (IB) of ENKD1 and α-tubulin in wild-type and *Enkd1* knockout mice.
D–F   Immunofluorescence images (D) and quantification of the density of cilia (E, $n = 20$ fields from three mice) and ciliary length (F, $n = 100$ cilia from three mice) in mouse retinas stained with antibodies against acetylated α-tubulin (Ace-α-tubulin) and γ-tubulin and DAPI. Scale bar, 2 μm.
G, H   ERG recording images (G) and a-b wave amplitudes (H, $n = 5$ mice) show the difference in the ERG a-b wave amplitude between wild-type and *Enkd1* knockout mice.
I, J   VEP recording images (I) and N2-P2 wave amplitudes (J, $n = 5$ mice) show the difference in the VEP N2-P2 wave amplitude between wild-type and *Enkd1* knockout mice.
K–M   Immunofluorescence images (K) and quantification of the percentage of ciliated cells (L, $n = 3$ mice) and ciliary length (M, $n = 100$ cilia from three mice) in mouse kidneys stained with the antibody against acetylated α-tubulin and DAPI. To quantify the percentage of ciliated cells (L), > 200 cells from 12 images were analyzed for each mouse. Scale bar, 3 μm.
N–Q   Images (N) and quantification of the percentage of flagellated sperm (O, $n = 9$ mice), flagellar length (P, $n = 100$ sperm from nine mice), and the percentage of sperm with normal motility among flagellated sperm (Q, $n = 9$ mice) for wild-type and *Enkd1* knockout mice. To quantify the percentage of flagellated sperm (O), > 200 sperm were analyzed for each mouse. To quantify the percentage of sperm with normal motility among flagellated sperm (Q), > 200 flagellated sperm were analyzed for each mouse. In panel N, the arrows indicate two spermatozoa without tails. Scale bar, 50 μm.
R, S   Scanning electron microscopy images of cilia (R) and quantification of the percentage of ciliated cells (S, $n = 9$ mice) in the mouse tracheal epithelium. To quantify the percentage of ciliated cells (S), > 200 cells from six fields were analyzed for each mouse. Scale bar, 5 μm.

Data information: Data are presented as mean ± SEM. Unpaired two-tailed *t*-test was performed. $P < 0.05$ (*), $P < 0.01$ (**), $P < 0.001$ (***), ns, not significant.
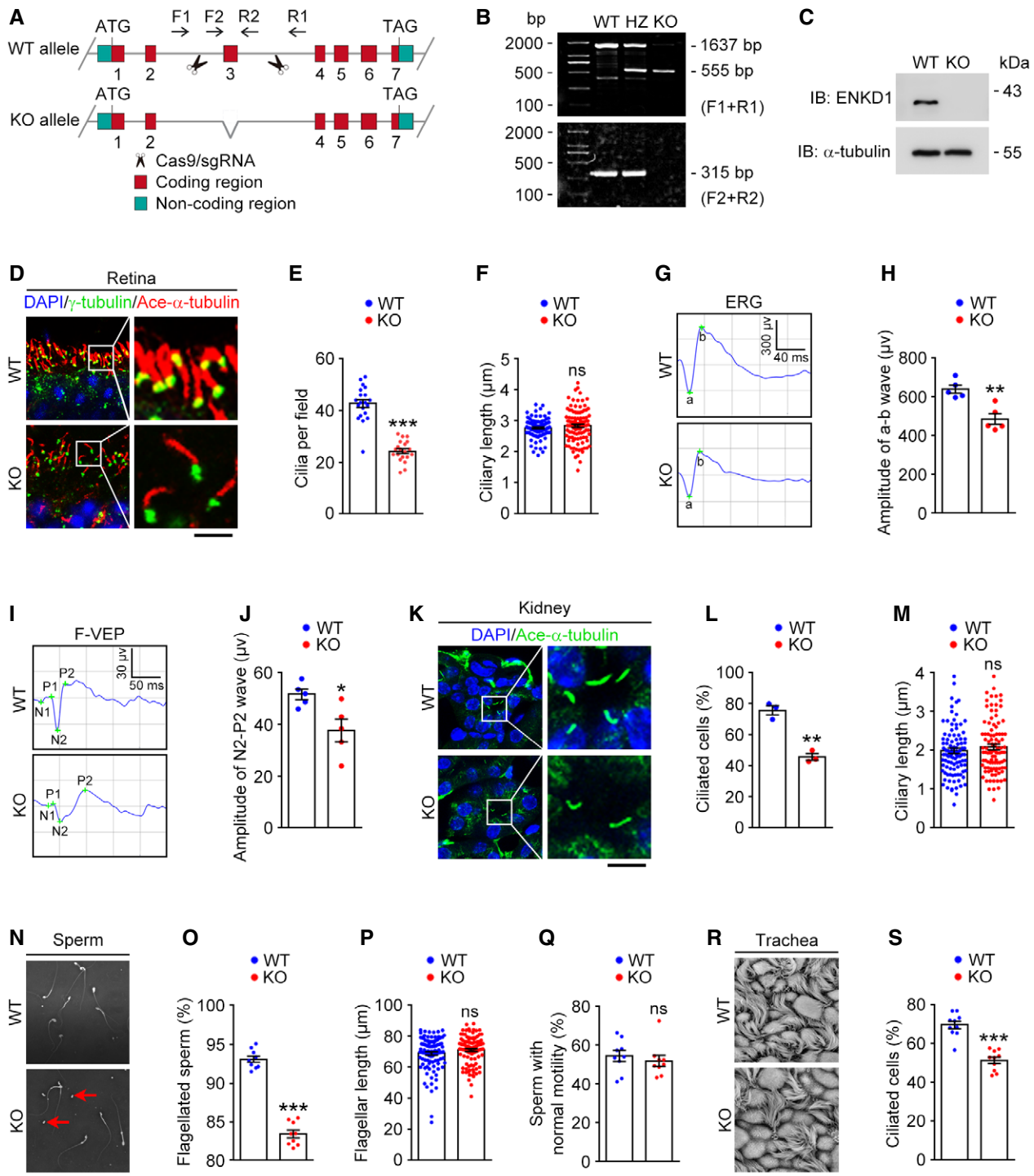
Figure 1.

unaffected male fertility of *Enkd1* knockout mice. We then analyzed cilia in the trachea by scanning electron microscopy and found that loss of ENKD1 significantly reduced the percentage of ciliated cells in the tracheal epithelium (Fig 1R and S). Further immunostaining revealed that quite a few CEP164-positive cells were non-multiciliated in *Enkd1* knockout mice (Fig EV1H and I), suggesting that ENKD1 depletion affects axoneme formation but not centriole amplification. Taken together, these results suggest that ENKD1 is required for the assembly of both primary and motile cilia.

ENKD1 is indispensable for the formation of primary cilia

To confirm the requirement of ENKD1 for ciliogenesis, we examined primary cilia in mouse embryonic fibroblasts (MEFs) isolated from

Enkd1 knockout mice. We found that *Enkd1* knockout MEFs had ciliogenesis defects similar to that observed in the tissues of *Enkd1* knockout mice (Fig 2A–D). Next, we knocked down ENKD1 in serum-starved human RPE1 cells by using two different siRNAs (Fig 2E), and found that downregulation of ENKD1 resulted in fewer cilia that were labeled with anti-acetylated α-tubulin and anti-Arl13b

antibodies (Fig 2F–J). Similarly, siRNA-mediated ENKD1 depletion did not affect the average length of existing cilia in RPE1 cells (Fig 2F and H), indicating that ENKD1 is largely dispensable for the elongation or disassembly of cilia. We further knocked down ENKD1 in serum-starved mouse NIH3T3 cells and observed similar results (Fig EV2A–D).
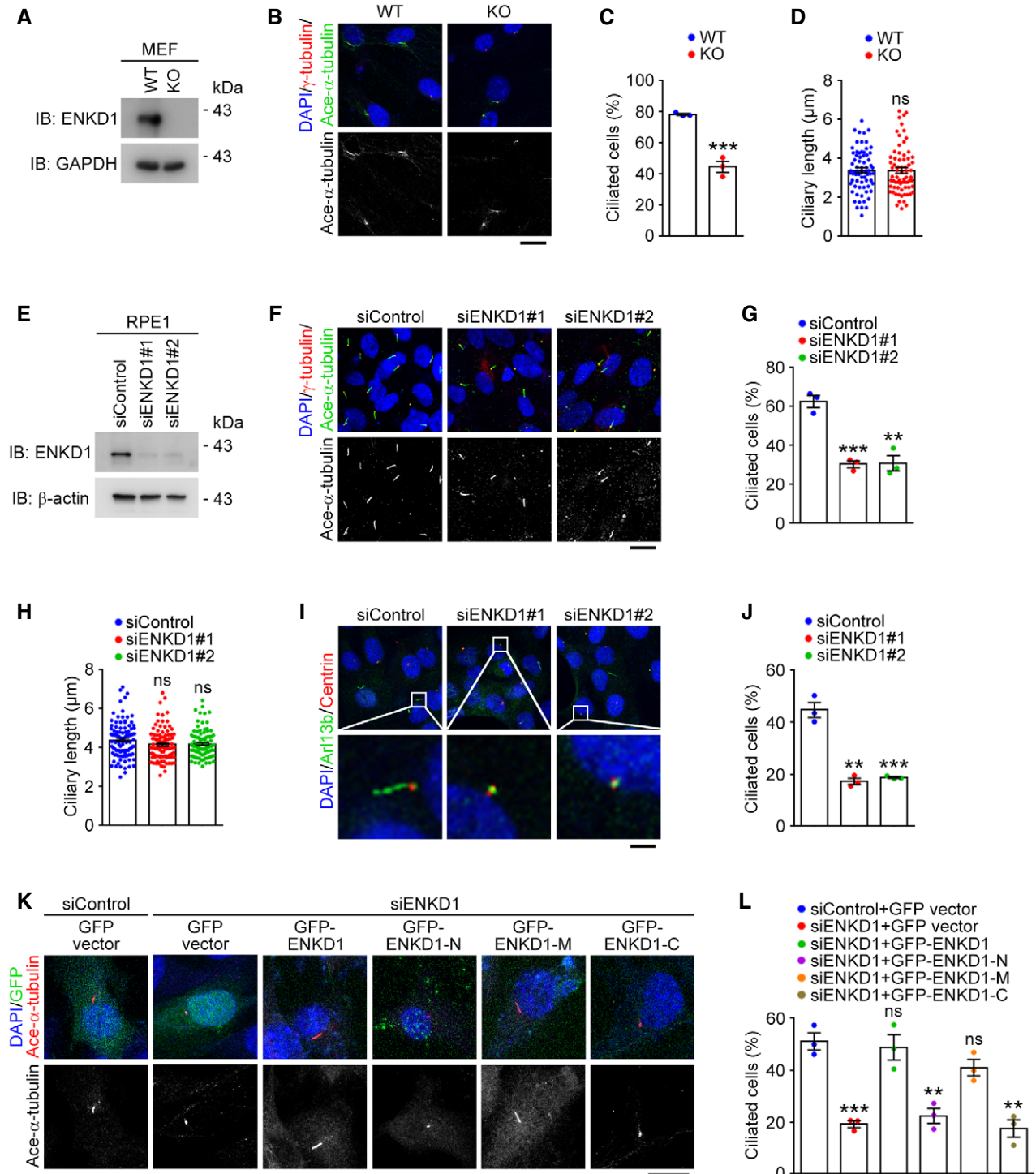

Figure 2.

To explore the potential molecular mechanism underlying ENKD1-mediated regulation of ciliogenesis, we constructed the ENKD1 expression plasmid as well as a series of truncated mutants of ENKD1, including ENKD1-N (1–91 amino acid [aa]), ENKD1-M (91–250 aa), and ENKD1-C (250–346 aa), which were based on the conserved domain analysis. The carboxyl-terminal fragment contains a conserved enkurin domain. Full-length ENKD1 or various truncated mutants of ENKD1 were re-expressed in ENKD1-knockdown RPE1 cells. We found that re-expression of full-length ENKD1 or ENKD1-M, but not ENKD1-N and ENKD1-C, significantly rescued ENKD1 siRNA-induced ciliogenesis defects (Fig 2K and L). Collectively, the above results reveal a critical role for the middle domain of ENKD1 in the initiation of ciliogenesis.

ENKD1 is a component of the centrosome

To further investigate the association of ENKD1 with ciliogenesis, we examined its subcellular localization. The comparison of antibody reactivity in MEFs isolated from wild-type or *Enkd1* knockout mice was performed to validate the antibody specificity. Immunostaining results revealed that ENKD1 displayed centrosomal localization in wild-type MEFs, which disappeared in *Enkd1* knockout MEFs (Fig EV3A). Similarly, ENKD1 knockdown dramatically decreased the centrosomal localization of ENKD1 but not the centrosomal marker Centrin (Fig EV3B–D). These results confirm the antibody specificity and demonstrate that ENKD1 is a component of the centrosome.

We further examined ENKD1 centrosomal localization and found that ENKD1 steadily localized at the centrosome and tended to accumulate at the parental centrioles during centriole duplication in cycling cells (Fig 3A). Considering that distal and subdistal appendages play essential roles in cilium formation and function (Vertii *et al*, 2016), we thus assessed the relative positions of ENKD1, CEP164, and Ninein. Fluorescence intensity profiles revealed that ENKD1 displayed a similar diameter to those of CEP164 and Ninein (Fig 3B and C). Since the centrosomal proteins that constitute the central region of the basal body are basically organized into ring structures (Gartenmann *et al*, 2017), we applied three-dimensional structural illumination microscopy (3D-SIM) to determine the radial

distances of different centrosomal proteins. Centrin was used to mark the central region of the basal body, and distances between Centrin and centriolar assembly proteins, including CEP192, CEP164, ENKD1, Ninein, and γ-tubulin, were analyzed. Consistent with the results of line scans, the diameter of the ENKD1 toroid is between the radius ranges of CEP164 and Ninein (Fig 3D–F), indicating that ENKD1 is localized near the outermost part of centrioles.

To explore ENKD1 localization dynamics under normal serum or serum-starved culture condition, RPE1 and NIH3T3 cells were cultured with or without serum and examined by immunofluorescence microscopy. We found that serum withdrawal had no obvious effects on the centrosomal localization of ENKD1 (Figs 3G and EV3E). In ciliated cells, ENKD1 was detected at the basal body of the cilium (Figs 3H and EV3F). Interestingly, we found that when overexpressed, ENKD1 not only localized to the basal body but also accumulated at the axoneme of cilia (Fig 3I). In addition, overexpression of ENKD1 induced the formation of microtubule bundles (Fig 3I). To determine how ENKD1 is recruited to the centrosome, we overexpressed truncated mutants of ENKD1, including ENKD1-N, ENKD1-M, and ENKD1-C in RPE1 cells. Although full-length and truncated ENKD1 displayed similar expression levels, ENKD1-M, but not ENKD1-N or ENKD1-C, was able to localize at the centrosome (Figs 3J and EV3G and H). Together, these results suggest that ENKD1 is localized to the centrosome through its middle domain.

3D-SIM analysis further showed that in cells under normal serum or serum-starved culture condition, ENKD1 formed ring-like structures at the mother and daughter centrioles (Fig 3K). The dynamics of ENKD1 localization at the centrosome during ciliogenesis were then examined, and no obvious changes were observed during the whole process of ciliogenesis (Fig 3K), suggesting that ENKD1 is a stable component of the centrosome.

ENKD1 functions in the removal of CP110 from the mother centriole

The centrosomal localization of ENKD1 suggests that it regulates ciliogenesis at an early stage. In mammalian cells, the formation of cilia involves a series of conserved early steps including centriole maturation into the basal body, ciliary vesicle formation, and CP110

removal (Sánchez & Dynlacht, 2016; Tu *et al*, 2018). To determine whether ENKD1 is involved in these processes, we examined the effect of ENKD1 knockdown on the localization of known complexes that play important roles in these steps (Fig 4A). We found that, in ENKD1-depleted cells, the localization of CEP192, PLK4,

CEP135, and CPAP at the centrosome was largely normal, indicating that ENKD1 is not essential for the structural integrity of the centrosome (Fig EV4A–H). Next, we tested the effect of ENKD1 knockdown on ciliary vesicle formation and found that, in ENKD1-depleted cells, CEP164 and Rab8a maintained their centriolar
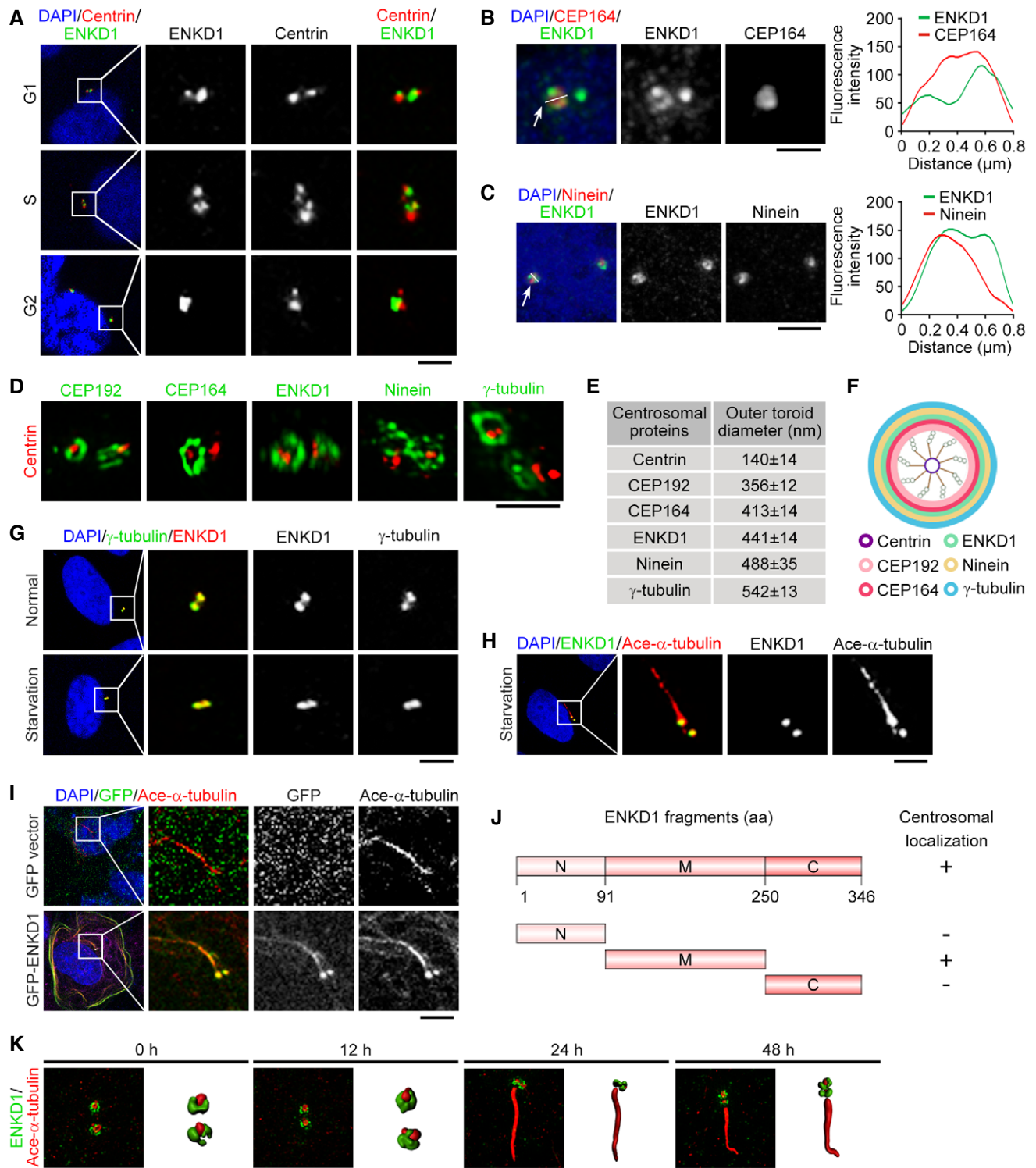

Figure 3.

Figure 3. ENKD1 is a component of the centrosome.

A   Immunofluorescence images of RPE1 cells cultured in normal serum medium, and stained with antibodies against ENKD1 and Centrin and DAPI. Scale bar, 1 μm.

B   Immunofluorescence images and fluorescence intensity profiles of ENKD1 and CEP164 in serum-starved RPE1 cells. The arrow marks the centriole subjected to the line scan. Scale bar, 1 μm.

C   Immunofluorescence images and fluorescence intensity profiles of ENKD1 and Ninein in serum-starved RPE1 cells. The arrow marks the centriole subjected to the line scan. Scale bar, 2 μm.

D–F   3D-SIM super-resolution images (D), quantification of the outer toroid diameters (E, *n* = 20 cells from three independent experiments), and a model illustrating the relative positions of γ-tubulin, Ninein, ENKD1, CEP164, CEP912, and Centrin (F) within a centriole. RPE1 cells were serum starved and stained with antibodies against the indicated proteins. Scale bar, 1 μm.

G   Immunofluorescence images of RPE1 cells cultured in normal serum or serum-free medium, and stained with antibodies against ENKD1 and γ-tubulin and DAPI. Scale bar, 1 μm.

H   Immunofluorescence images of RPE1 cells cultured in serum-free medium, and stained with antibodies against ENKD1 and acetylated α-tubulin and DAPI. Scale bar, 1 μm.

I   Immunofluorescence images of RPE1 cells transfected with GFP-ENKD1 or GFP vector, cultured in a serum-starved condition, and stained with the antibody against acetylated α-tubulin and DAPI. Scale bar, 1 μm.

J   Schematic diagrams showing the centrosomal localization domain of ENKD1.

K   3D-SIM images of ENKD1 localization at the centrosome in RPE1 cells cultured in serum-free medium (0, 12, 24, or 48 h of serum starvation), and stained with antibodies against ENKD1 and acetylated α-tubulin. Scale bar, 1 μm.

Data information: Data are from three independent biological repeats and presented as mean ± SD.

localization (Fig EV4I–L), suggesting that ENKD1 is dispensable for ciliary vesicle formation.

Next, we examined the centrosomal localization of two key negative regulators of ciliogenesis, CP110 and CEP97. Previous studies have shown that the removal of these two proteins from the mother centriole is essential for the initiation of ciliogenesis (Kobayashi *et al*, 2011). We found that, upon ENKD1 depletion, the percentage of cells with strong CP110 and CEP97 signals at both mother and daughter centrioles was significantly increased (Fig 4B–E), suggesting a function of ENKD1 in the removal of CP110 and CEP97 from the mother centriole. Furthermore, we evaluated the long-term effects of ENKD1 depletion on CP110 removal by a 120-h knockdown of ENKD1 expression in RPE1 cells. Interestingly, more cells were observed to have one CP110 dot in the 120-h knockdown group (Fig 4F–H) compared to the 48-h knockdown group (Fig 4C). These results indicate that CP110 is able to be removed from the mother centriole inefficiently in an ENKD1-independent way.

ENKD1 regulates the CP110–CEP97 interaction

We next asked how ENKD1 regulates the removal of CP110 from the mother centriole. Since M-phase phosphoprotein 9 (MPP9) has

been reported to regulate the removal of the CP110–CEP97 complex during ciliogenesis (Huang *et al*, 2018), we sought to test whether and how ENKD1 is involved in the MPP9-mediated CP110 removal. Interestingly, we observed a mild increase in the percentage of cells with one CP110 dot in ENKD1 and MPP9 co-depleted cells as compared to that in ENKD1-depleted cells (Fig 5A–C). Moreover, ENKD1 depletion significantly suppressed the CP110 removal caused by MPP9 depletion (Fig 5C). Overall, these results suggest that ENKD1- and MPP9-dependent pathways co-exist to ensure the mother centriole uncapping during ciliogenesis, and ENKD1 also functions downstream of the MPP9-dependent CP110 removal.

To corroborate the role of CP110 in ENKD1-mediated ciliogenesis, we knocked down the expression of CP110 by specific siRNAs in ENKD1-depleted RPE1 cells. We found that CP110 knockdown significantly rescued the ciliary defects caused by ENKD1 depletion (Fig 5D–F). Given the vital role of CP110 in controlling centriole length (Spektor *et al*, 2007; Schmidt *et al*, 2009), we sought to investigate the effects of ENKD1 depletion on centriole length. By staining with either anti-Centrin or anti-acetylated α-tubulin antibodies, we found that centrioles maintained a similar length in control and ENKD1-depleted cells (Figs 2I and EV5A and B), suggesting a specific role for ENKD1 in regulating the removal of CP110 during ciliogenesis. Since the CP110–CEP97 interaction is crucial for capping the

Figure 4. ENKD1 functions in the removal of CP110 from the mother centriole.

A   A table summarizing the centrosomal localization of cilium-related proteins in ENKD1-depleted RPE1 cells.

B, C   Immunofluorescence images (B) and quantification of the percentage of cells with one CP110 dot (C, *n* = 3 independent experiments) for RPE1 cells transfected with control or ENKD1 siRNAs, cultured in serum-free medium, and stained with antibodies against CP110 and acetylated α-tubulin and DAPI. To quantify the percentage of cells with one CP110 dot (C), > 120 cells were analyzed for each experiment. Scale bar, 1 μm.

D, E   Immunofluorescence images (D) and quantification of the percentage of cells with one CEP97 dot (E, *n* = 3 independent experiments) for RPE1 cells transfected with control or ENKD1 siRNAs, cultured in serum-free medium, and stained with antibodies against CEP97 and acetylated α-tubulin and DAPI. To quantify the percentage of cells with one CEP97 dot (E), > 150 cells were analyzed for each experiment. Scale bar, 1 μm.

F–H   Immunoblot analysis (F), immunofluorescence images (G), and quantification of the percentage of cells with one CP110 dot (H, *n* = 3 independent experiments) for RPE1 cells transfected with control or ENKD1 siRNAs, cultured in serum-free medium for 120 h, and stained with antibodies against CP110 and acetylated α-tubulin and DAPI. To quantify the percentage of cells with one CP110 dot (C), > 80 cells were analyzed for each experiment. Scale bar, 1 μm.

Data information: Data are from three independent biological repeats and presented as mean ± SEM. Unpaired two-tailed *t*-test was performed. *P* < 0.01 (**), *P* < 0.001 (***).

Figure 4.

centrioles (Spektor *et al*, 2007), we performed immunoprecipitation assays to test whether ENKD1 is involved in regulating the CP110–CEP97 interaction. We found that the interaction between CP110 and CEP97 was significantly enhanced in the retinal tissues of *Enkd1* knockout mice (Fig 5G and H). Similar effect was observed in cultured RPE1 cells transfected with ENKD1-specific siRNAs (Fig 5I and J). Taken together, these data suggest that ENKD1 destabilizes the

CP110–CEP97 interaction, which in turn promotes the removal of CP110 and CEP97 from the mother centriole.

ENKD1 competes with CEP97 in binding to CP110

To understand the mechanism of ENKD1-mediated CP110 removal, we examined whether ENKD1 interacts with CP110 by
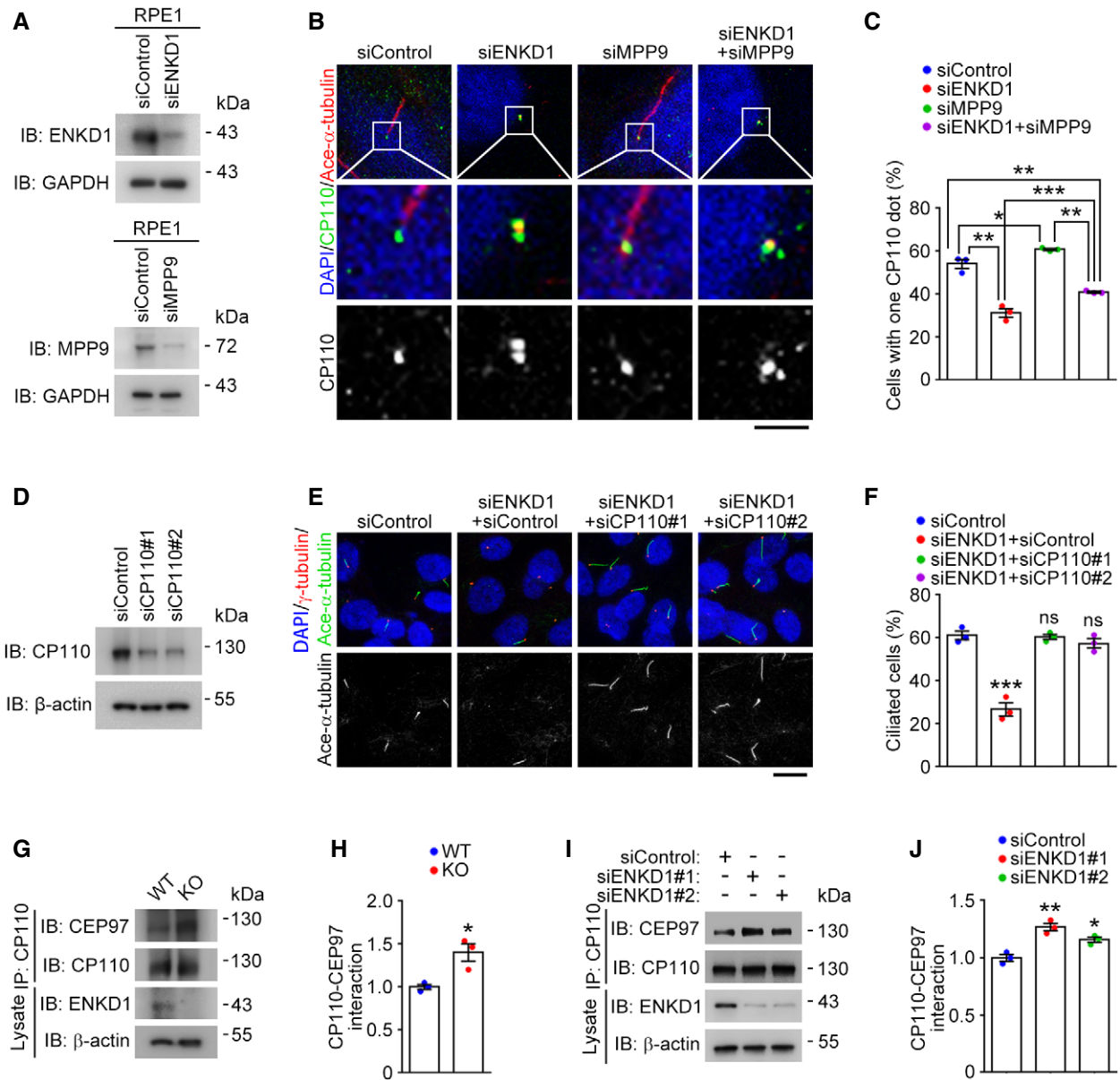
Figure 5. ENKD1 regulates the CP110–CEP97 interaction.

A–C   Immunoblot analysis (A), immunofluorescence images (B), and quantification of the percentage of cells with one CP110 dot (C, *n* = 3 independent experiments) for RPE1 cells transfected with the indicated siRNAs, cultured in serum-free medium for 48 h, and stained with antibodies against CP110 and acetylated α-tubulin and DAPI. To quantify the percentage of cells with one CP110 dot (C), > 180 cells were analyzed for each experiment. Scale bar, 1 μm.

D   Immunoblot analysis of CP110 and β-actin in RPE1 cells transfected with control or CP110 siRNAs and cultured in serum-free medium for 48 h.

E, F   Immunofluorescence images (E) and quantification of the percentage of ciliated cells (F, *n* = 3 independent experiments) for RPE1 cells transfected with the indicated siRNAs, cultured in a serum-starved condition, and stained with antibodies against γ-tubulin and acetylated α-tubulin and DAPI. To quantify the percentage of ciliated cells (F), >120 cells were analyzed for each experiment. Scale bar, 10 μm.

G, H   Immunoprecipitation and immunoblotting (G) and quantification (H, *n* = 3 mice) showing the CP110–CEP97 interaction in the retinal tissues of wild-type and *Enkd1* knockout mice. The intensity of each CEP97 band was normalized to that of the β-actin band.

I, J   Immunoprecipitation and immunoblotting (I) and quantification (J, *n* = 3 independent experiments) showing the CP110–CEP97 interaction in serum-starved RPE1 cells transfected with control or ENKD1 siRNAs. The intensity of each CEP97 band was normalized to that of the β-actin band.

Data information: Data are from three independent biological repeats and presented as mean ± SEM. Unpaired two-tailed *t*-test was performed. *P* < 0.05 (*), *P* < 0.01 (**), *P* < 0.001 (***), ns, not significant.
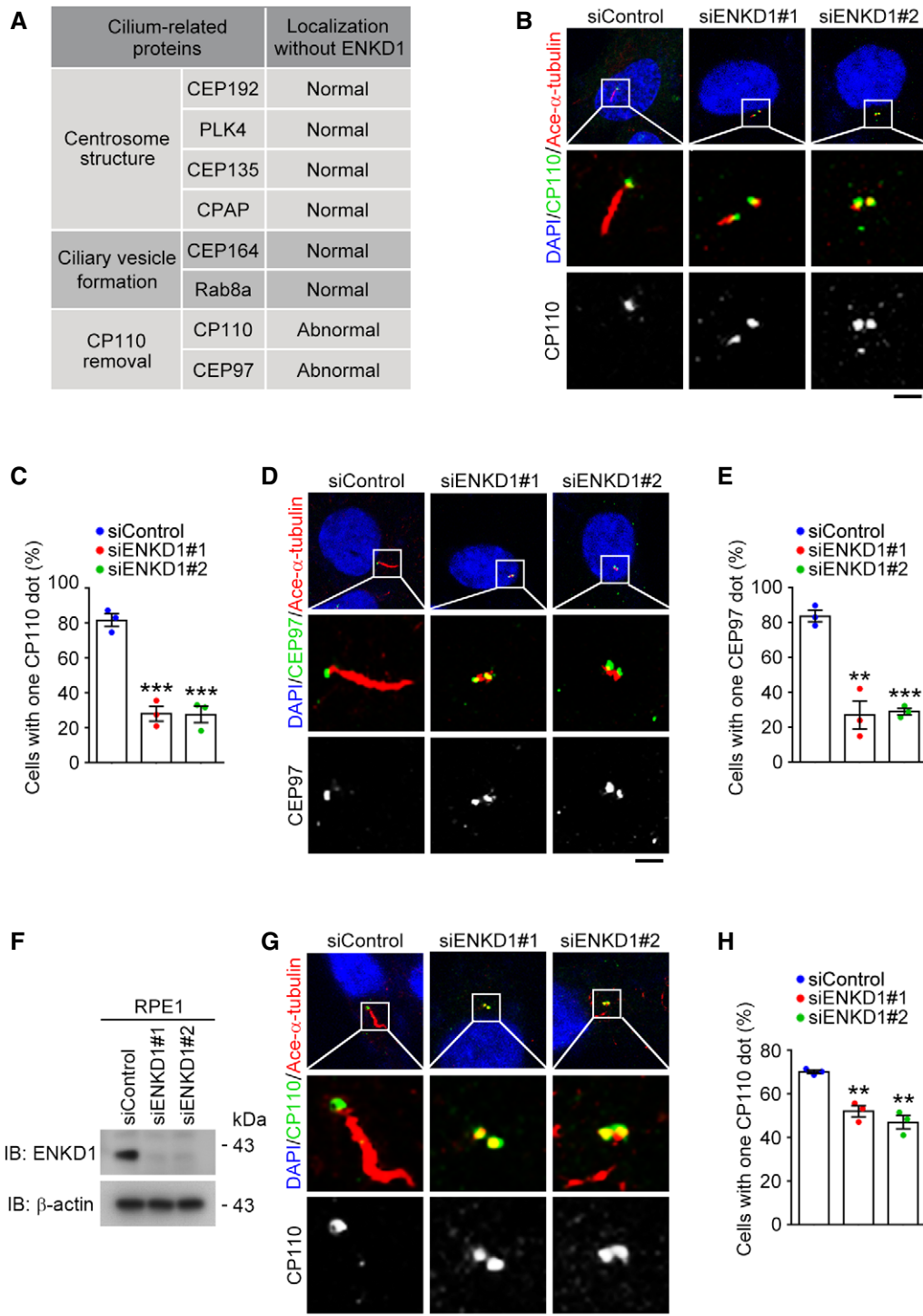
immunoprecipitation assays. We found that endogenous ENKD1 bound to CP110 in the lysate of mouse retinal tissues (Fig 6A). Next, we validated the interaction between ENKD1 and CP110 by using

the overexpression system. Immunoprecipitation assays showed that overexpressed GFP-ENKD1 was able to interact with both Flag-CP110 and HA-CP110 in HEK293T human embryonic kidney
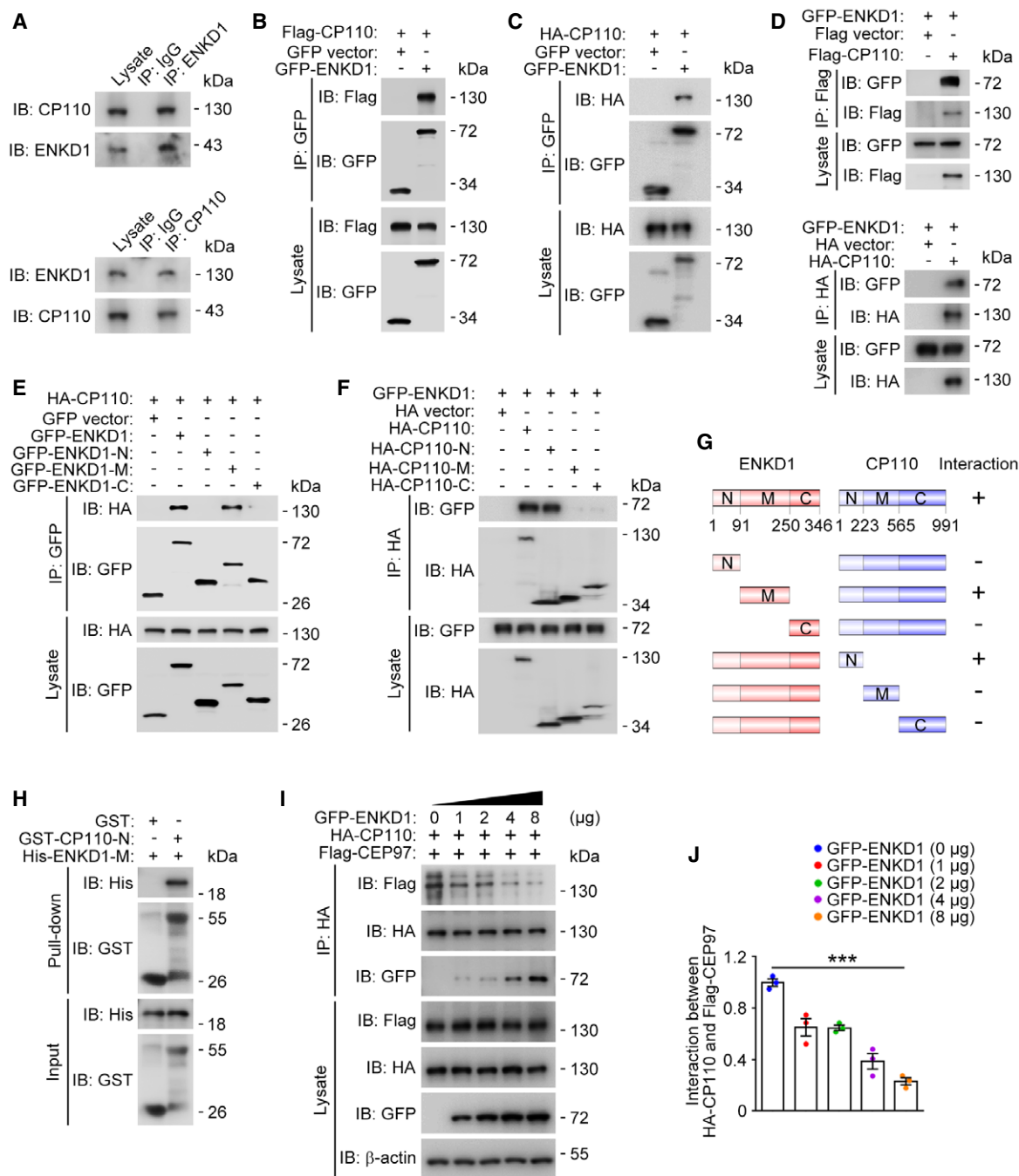
Figure 6. ENKD1 competes with CEP97 in binding to CP110.

A   Immunoprecipitation and immunoblotting showing the interaction between endogenous ENKD1 and CP110 in mouse retinal tissues. Immunoprecipitation was performed with the anti-ENKD1 (upper panel) or anti-CP110 (lower panel) antibody or the corresponding control IgG.

B–D   Immunoprecipitation and immunoblotting showing the interaction of GFP-ENKD1 with Flag-CP110 (B and upper panel of D) or HA-CP110 (C and bottom panel of D) in HEK293T cells. Immunoprecipitation was performed with antibodies against GFP (B and C), Flag (upper panel of D), or HA (bottom panel of D).

E   Identification of the domains of ENKD1 mediating its interaction with CP110.

F   Identification of the domains of CP110 mediating its interaction with ENKD1.

G   Schematic diagrams showing the domains of ENKD1 and CP110 that mediate their interaction.

H   GST pull-down showing the interaction of purified GST-CP110-N with purified His-ENKD1-M.

I, J   Immunoprecipitation and immunoblotting (I) and quantification (J, $n = 3$ independent experiments) showing the interaction of HA-CP110 with Flag-CEP97 in HEK293T cells transfected with the indicated plasmids. The intensity of each Flag-CEP97 band was normalized to that of the β-actin band.

Data information: Data are from three independent biological repeats and presented as mean ± SEM. Non-parametric one-way ANOVA analysis was performed. $P < 0.001$ (***).

epithelial cells (Fig 6B–D), demonstrating a strong interaction between ENKD1 and CP110.

Next, we sought to map the interaction domains in ENKD1 and CP110. Through a series of immunoprecipitation assays, we found that ENKD1 interacted with CP110 through its 91–250 aa region (Fig 6E and G), which is also responsible for the centrosomal localization of ENKD1 (Fig 3E). Immunoprecipitation assays with a series of truncated mutants of CP110 showed that the 1–223 aa domain of CP110 was sufficient for its interaction with ENKD1 (Fig 6F and G). A previous study demonstrated that the 1–223 aa domain of CP110 is essential for its interaction with CEP97 (Spektor et al, 2007). We next performed GST pull-down analysis using purified proteins to determine whether ENKD1 and CP110 could interact directly. We found that purified His-tagged ENKD1 middle fragment was able to interact with purified GST-tagged CP110 amino-terminal fragment, but not GST (Fig 6H), indicative of a direction interaction between ENKD1 and CP110. To investigate the relative strength of the interaction of CP110 with ENKD1 and CEP97, we performed competition experiments with constant amounts of HA-CP110 and Flag-CEP97, and increasing amounts of GFP-ENKD1. Interestingly, increasing amounts of ENKD1 caused a gradual decrease in the interaction between CEP97 and CP110 (Fig 6I and J). Collectively, these findings suggest that ENKD1 competes with CEP97 in binding to CP110 at the centrosome.

Discussion

The present study identifies the enkurin domain-containing protein ENKD1 as a novel regulator of cilium formation. The Enkurin protein (ENKUR) is known to interact with several transient receptor potential channel (TRPC) proteins, co-localize with these channel proteins in sperm, and participate in the initiation of fertilization. In addition, ENKUR has been demonstrated to regulate the formation of motile cilia to mediate the left–right axis patterning in vertebrates, but is not required for the assembly of primary cilia (Sigg et al, 2017). However, we found that, unlike ENKUR, ENKD1 is required for the proper assembly of both primary and motile cilia. Moreover, the middle region of ENKD1, but not its enkurin domain, is responsible for its centrosomal localization and interaction with CP110. These findings suggest that the enkurin domain is dispensable for the role of ENKD1 in ciliogenesis and that ENKD1 and enkurin participate in the regulation of cilia through different pathways.

Centrioles play essential roles in centrosomal structures and functions, including the ability to nucleate cilia (Kong et al, 2020; Yu et al, 2020). CP110 is known to positively regulate centriole duplication, restrict centriole length in S phase, and function as a negative regulator of ciliogenesis in G0/G1 phase (Chen et al, 2002; Tsang & Dynlacht, 2013). However, CP110 not only inhibits cilium formation but also localizes to centrosomal rootlets and regulates the ciliary adhesion complex for proper multiciliogenesis in Xenopus multiciliated cells (Song et al, 2014; Walentek et al, 2016). Thus, the cellular CP110 level has to be strictly controlled for each of the above process. During centriole duplication in S phase, CP110 is concentrated at the distal end of each procentriole and forms a complex with CEP97 to cap the centriole. However, CP110 must be removed from the distal end of the mother centriole, which is a prerequisite for the onset of ciliogenesis during G0/G1 phase. The

uncapping of the mother centriole's distal end is regulated by either downregulation of CP110 or removal of CP110 from the mother centriole (Cao et al, 2012; Goetz et al, 2012; Loukil et al, 2017; Huang et al, 2018).

At the initial stages of ciliogenesis, tau tubulin kinase 2 (TTBK2), a microtubule plus end-tracking kinase, was recruited to the distal end of the mother centriole by CEP164 (Čajánek & Nigg, 2014), where it phosphorylates MPP9 and mediates the degradation of MPP9 (Huang et al, 2018). Since MPP9 is believed to anchor the CP110–CEP97 complex to the distal end of the mother centriole, the degradation of MPP9 facilitates the removal of the CP110–CEP97 complex from the mother centriole (Huang et al, 2018). However, the localization of CP110 at the daughter centriole is not affected by the depletion of MPP9, although MPP9 also co-localizes with CP110 and CEP97 at the daughter centriole (Huang et al, 2018), suggesting that there exist other pathways that may also contribute to the delocalization of CP110 at the mother centriole during ciliogenesis.

The present study reveals a novel molecular pathway controlling the removal of the CP110–CEP97 complex from the mother centriole during cilium formation. CEP97 is known to interact with CP110, and CEP97 depletion can cause the disappearance of CP110 from both mother and daughter centrioles, indicating that the CP110–CEP97 interaction is crucial for the localization of CP110 to centrioles (Spektor et al, 2007). Our results show that ENKD1 can interact with the amino-terminal region of CP110, which is known to mediate the interaction of CP110 with CEP97 (Spektor et al, 2007). In addition, our data demonstrate that depletion of ENKD1 strengthens the CP110–CEP97 interaction. Taken together, these findings indicate that ENKD1 may disrupt the CP110–CEP97 interaction via competitively binding to CP110, which may in turn destabilize or release CP110 and further stimulate the initiation of ciliogenesis. It will be interesting to investigate in the future how ENKD1 is precisely regulated to compete with CEP97 in interacting with CP110 during ciliogenesis.

Materials and Methods

Enkd1 knockout mice

Enkd1 knockout mice were generated with the CRISPR/Cas9 technology. In brief, sgRNAs were transcribed in vitro, and Cas9 proteins and sgRNAs were co-microinjected into the fertilized eggs of C57BL/6J mice. Fertilized eggs were transplanted to obtain positive F0 mice, which were confirmed by PCR and sequencing. F1 mice were obtained by mating positive F0 mice with C57BL/6J mice. Enkd1 knockout mice were identified by PCR with the following primers: forward primer 1 (F1: 5′-TGCCTTGAGCCCATGCAGTT-3′), reverse primer 1 (R1: 5′-GCTCAGGAGGTGGACAAAGGAG-3′), forward primer 2 (F2: 5′-TGGCAGGATCAGAGTCTATCCTTC-3′), and reverse primer 2 (R2: 5′-GCCTCCAACTGTGACTCCCATAC-3′). Mice were housed in a temperature-controlled facility with a 12-h light/ 12-h dark cycle, specific pathogen-free environment, and provided with food and water. All mouse experiments were carried out in accordance with the relevant regulatory standards and were approved by the Animal Care and Use Committee of Shandong Normal University.

Neither randomization nor blinding was applied for animal studies.

Antibodies

The following primary antibodies were used: rabbit anti-ENKD1 (Abcam, ab224560; IF 1:500), rabbit anti-Rab8a (Abcam, ab188574; IF 1:500), mouse anti-α-tubulin (Abcam, ab7291; IB 1:1,000), rabbit anti-ENKD1 (Sigma-Aldrich, HPA041478; IB 1:1,000), mouse anti-γ-tubulin (Sigma-Aldrich, T6557; IF 1:1,000), rabbit anti-γ-tubulin (Sigma-Aldrich, T3320; IF 1:1,000), mouse anti-acetylated α-tubulin (Sigma-Aldrich, T7451; IF 1:1,000), mouse anti-acetylated α-tubulin (Sigma-Aldrich, T6793; IF 1:500), mouse anti-Centrin (Millipore, 04-1624; IF 1:1,000), mouse anti-CEP164 (Santa Cruz Biotechnology, sc-515403; IF 1:500), mouse anti-Ninein (Santa Cruz Biotechnology, sc-376420; IF 1:500), rabbit anti-CEP164 (Protein-tech, 22227-1-AP; IF 1:1,000), rabbit anti-CP110 (Proteintech, 12780-1-AP; IF 1:1,000; IB 1:1,000), rabbit anti-CEP192 (Proteintech, 18832-1-AP; IF 1:1,000), rabbit anti-Centrin (Proteintech, 12794-1-AP; IF 1:500), rabbit anti-PLK4 (Proteintech, 12952-1-AP; IF 1:500), rabbit anti-CPAP (Proteintech, 11517-1-AP; IF 1:500), rabbit anti-CEP135 (Proteintech, 24428-1-AP; IF 1:500), rabbit anti-CEP97 (Proteintech, 22050-1-AP; IF 1:1,000; IB 1:1,000), rabbit anti-MPP9 (Abways, AY3035; IB 1:500), rabbit anti-β-actin (Abways, AB0035; IB 1:2,000), rabbit anti-GAPDH (Abways, AB0036; IB 1:2,000), rabbit anti-GFP (Abways, AB0045; IF 1:2,000; IB 1:1,000), mouse anti-HA tag (Abways, AB0004; IB 1:1,000), mouse anti-Flag tag (Abways, AB0008; IB 1:1,000), mouse anti-GST tag (Abways, AB0003; IB 1:1,000), and mouse anti-His tag (Abways, AB0002; IB 1:1,000). Alexa Fluor 488- or 568-conjugated secondary antibodies were purchased from Life Technologies. Horseradish peroxidase-conjugated secondary antibodies were obtained from Abways.

Cell culture

RPE1 cells (ATCC) were cultured in DMEM/F12 medium containing 10% fetal bovine serum (FBS, GBICO), penicillin, and streptomycin. NIH3T3, HEK293T, and U2OS cells (ATCC) were cultured in DMEM medium supplemented with 10% FBS, penicillin, and streptomycin. Mouse embryonic fibroblasts (MEFs) were isolated and cultured as previously described (Xu, 2005). All cell lines were cultured at 37°C with 5% CO_2. To induce cilium formation, cells were cultured in serum-free medium for 48 h unless stated otherwise.

Transfection of plasmids and siRNAs

Mammalian expression plasmids for GFP-ENKD1, Flag-CP110, and HA-CP110 were constructed by using the pEGFP-C1, pEnter, and pCMV-C-HA vectors, respectively (Table EV1). Various truncated mutants were constructed by PCR. The siRNA-resistant forms of ENKD1 were constructed for rescue experiments. All plasmids were verified by DNA sequencing. To transfect plasmids into RPE1 cells, Lipofectamine 3000 (Thermo Fisher Scientific) was used following the manufacturer's instructions. For HEK293T cell transfection, cells were seeded in plates in DMEM with 10% FBS and without antibiotics. After cell adherence, the transfection mixture containing plasmids and polyethylenimine (Polyscience) was added into the culture medium. The medium was changed to fresh DMEM with 10% FBS

12 h after transfection. To knockdown the expression of endogenous proteins, the following siRNAs were synthesized by GenePharma: control (siControl: 5′-CGUACGCGGAAUACUUCGA-3′); human ENKD1 (siENKD1#1: 5′-GUGGACUUCAUUCGUCACATT-3′; siENKD1#2: 5′-GGCCCAAAGUCUUCGUGAATT-3′); mouse ENKD1 (siENKD1#a: 5′-GGCGGAUCAAAGAGAUUCATT-3′; siENKD1#b: 5′-C ACCCAAGUAUGACA AUGUTT-3′); human CP110 (siCP110#1: 5′-AA GCAGCAUGAGUAUGCCAGU-3′; siCP110#2: 5′-UAGACUUAUGCAGA CAGAUAA-3′); and human MPP9 (5′- CGCUAAAGAAAUUCCAUGUU TT-3′). Cells were transfected with siRNAs by using Lipofectamine RNAiMAX (Thermo Fisher Scientific) following the manufacturer's instructions. All transfections were performed in a serum-free culture condition.

Immunoprecipitation and immunoblotting

Samples were lysed in a lysis buffer (50 mM Tris–HCl, 150 mM NaCl, 1 mM EDTA, 3% glycerinum, and 1% NP-40, pH 7.5) with a protease inhibitor cocktail (Thermo Fisher Scientific). For immuno-precipitation, cell lysates were incubated for 8 h at 4°C with anti-GFP (MBL, D153-8), anti-HA (Sigma-Aldrich, A2095), anti-Flag beads (Abmart, M20018), or protein A/G beads (Thermo Scientific, 20421) pre-incubated with primary antibodies. The beads were then washed with the lysis buffer. Samples were denatured and separated by SDS–PAGE. Proteins were then transferred onto polyvinylidene difluoride membranes, which were blocked with 5% fat-free milk at room temperature for 2 h and incubated with primary antibodies overnight at 4°C. The membranes were then incubated with horse-radish peroxidase-conjugated secondary antibodies (1: 5,000) for 1 h at room temperature. Protein bands were visualized by using the luminol reagent (Millipore).

GST pull-down

GST-CP110 (1–223 aa, named GST-CP110-N) and His-ENKD1 (91–250 aa, named His-ENKD1-M) proteins were expressed in *E. coli* and purified with glutathione resins (GenScript, L00206) or Ni-NTA resins (Thermo Scientific, 88221). To perform GST pull-down, 100 μg of GST or GST-CP110-N fusion protein was immobilized with 50 μl of glutathione resins in 1 ml lysis buffer by incubating at 4°C for 4–6 h with gentle rocking motion. Beads were washed three times with the lysis buffer and incubated with 100 μg of His-ENKD1-M protein overnight at 4°C with gentle rotation. The bound proteins were eluted with loading buffer and analyzed by immunoblotting.

Immunofluorescence microscopy

Mouse eye tissues were fixed in 4% paraformaldehyde in phosphate-buffered saline (PBS) for 30 s at room temperature, and then cryo-embedded in Tissue-Tek OCT (Sakura) on dry-ice slabs. Mouse kidney tissues were fixed in 4% paraformaldehyde in PBS at 4°C overnight, and then cryo-embedded in Tissue-Tek OCT (Sakura) on dry-ice slabs. Frozen sections were cut into 10 mm slices on a Leica CM1950 cryostat and mounted on Superfrost Plus slides (Thermo Fisher Scientific). Thin sections were pre-permeabilized in 0.3% Triton X-100/PBS for 1 min, fixed with 4% paraformaldehyde for 20 min, and permeabilized in 0.5% Triton X-100/PBS for 20 min.

The tissues were then blocked in 4% bovine serum albumin (BSA) for 1 h and stained with primary antibodies at 4°C overnight. They were then stained with secondary antibodies and DAPI (Sigma-Aldrich). The sections were subsequently mounted onto slides and examined with a Leica SP8 confocal microscope. For cultured cells, cells grown on glass coverslips were fixed in ice-cold methanol for 3 min, and then washed with PBS. Cells were blocked with 4% BSA in PBS for 1 h at room temperature, incubated with primary antibodies for 2 h, and then with secondary antibodies for 1 h. Finally, cells were stained with DAPI for 5 min and examined under a microscope. The length of cilia, the percentage of ciliated cells, and the diameter of centrosome toroids were measured with Image J (National Institutes of Health). The fluorescence intensity of centrosomal proteins was measured with the Fiji software (National Institutes of Health).

ERG and F-VEP recordings

ERG and F-VEP were measured with a visual electrophysiological instrument (BeiJing Health OLight Technology, OPTO-III). Briefly, after overnight dark adaptation, mice were anesthetized with a mixture of ketamine (100 mg/kg body weight) and xylazine (10 mg/kg body weight). The pupils were dilated with 0.5% tropicamide phenylephrine ophthalmic solution. For ERG analysis, the reference electrode was placed in the mouse tail, the recording electrode on the head, and the loop electrode in contact with the central cornea. ERG responses were recorded according to the instrument operation manual. To detect F-VEP, a needle electrode, which served as the recording electrode, was inserted subcutaneously over the visual cortex, a reference electrode was placed 5 mm above the nasal root, and a third electrode was placed in the tail and served as the ground. Visually evoked potentials from mice were recorded individually.

ECG analysis

Mice at 3 months old were anesthetize and placed on the ECG platform with their abdomen facing up, and measured by an ECG system (AD Instruments, Quad Bridge Amp ML224). Three electrodes were connected to the sensors; two of them were placed on the right front paw and left front paw of the mice, as negative and positive poles, respectively, and the third electrode was placed on the left hind paw as a neutral wire. RR intervals were recorded using the ECG system and analyzed with the LabChart software V8 (AD Instruments).

Sperm analysis

The cauda epididymis was isolated from mice, immersed in normal saline, and cut into pieces. Samples were incubated at 37°C for 15 min to allow sperm to escape from the epididymis. Sperm motility was examined on a TV monitor, which was connected to a camera mounted onto a phase-contrast microscope (AndroVision, Minitube, Germany). Images were captured at 50 frames per second. The number and length of sperm were analyzed with ImageJ.

Electron microscopy

For scanning electron microscopy, mouse tracheal tissues were isolated and fixed with 2.5% glutaraldehyde in 0.1 M PBS at 4°C overnight. Samples were post-fixed in 1% osmium tetroxide for 1 h, dehydrated in ethanol gradient buffer, and dried by critical point drying. The samples were then gold coated by the sputter technique and examined with a scanning electron microscope (Hitachi Asia Ltd, TM3030) at an accelerating voltage of 15 kV.

Statistical analysis

GraphPad Prism (GraphPad Software) was used for statistical analysis. Experiments were performed three times unless stated otherwise. Statistical results were shown as means ± SEM unless indicated otherwise. Significant differences between two groups were analyzed using the unpaired two-tailed *t*-test. For multiple-condition comparisons, non-parametric one-way ANOVA analysis was performed.

Data availability

No data from this study are deposited in external repositories.

Expanded View for this article is available online.

Author contributions

Ting Song: Data curation; Validation; Investigation; Methodology; Writing—original draft; Writing—review & editing. **Yunfan Yang:** Formal analysis; Investigation. **Peng Zhou:** Investigation. **Jie Ran:** Investigation. **Liang Zhang:** Investigation; Methodology. **Xiaofan Wu:** Investigation. **Wei Xie:** Investigation. **Tao Zhong:** Investigation. **Hong-Bin Liu:** Formal analysis. **Min Liu:** Formal analysis. **Dengwen Li:** Data curation; Formal analysis. **Huijie Zhao:** Data curation; Formal analysis; Writing—review & editing. **Jun Zhou:** Conceptualization; Data curation; Formal analysis; Supervision; Funding acquisition; Writing—original draft; Writing—review & editing.

In addition to the CRediT author contributions listed above, the contributions in detail are:
TS and JZ designed the experiments. TS, PZ, JR, LZ, XW, WX, and TZ performed the experiments. TS, YY, HL, ML, DL, HZ, and JZ analyzed data. TS, YY, HZ, and JZ wrote the manuscript. JZ supervised the project.

Disclosure and competing interests statement
The authors declare that they have no conflict of interest.

References

Anvarian Z, Mykytyn K, Mukhopadhyay S, Pedersen LB, Christensen ST (2019) Cellular signalling by primary cilia in development, organ function and disease. *Nat Rev Nephrol* 15: 199–219

Bettencourt-Dias M, Carvalho-Santos Z (2008) Double life of centrioles: CP110 in the spotlight. *Trends Cell Biol* 18: 8–11

Buskin A, Zhu L, Chichagova V, Basu B, Mozaffari-Jovin S, Dolan D, Droop A, Collin J, Bronstein R, Mehrotra S *et al* (2018) Disrupted alternative splicing for genes implicated in splicing and ciliogenesis causes PRPF31 retinitis pigmentosa. *Nat Commun* 9: 4234

Čajánek L, Nigg EA (2014) Cep164 triggers ciliogenesis by recruiting Tau tubulin kinase 2 to the mother centriole. *Proc Natl Acad Sci USA* 111: E2841–2850

Cao J, Shen Y, Zhu L, Xu Y, Zhou Y, Wu Z, Li Y, Yan X, Zhu X (2012) miR-129-3p controls cilia assembly by regulating CP110 and actin dynamics. *Nat Cell Biol* 14: 697–706

Carvalho-Santos Z, Machado P, Branco P, Tavares-Cadete F, Rodrigues-Martins A, Pereira-Leal JB, Bettencourt-Dias M (2010) Stepwise evolution of the centriole-assembly pathway. *J Cell Sci* 123: 1414–1426

Chen Z, Indjeian VB, McManus M, Wang L, Dynlacht BD (2002) CP110, a cell cycle-dependent CDK substrate, regulates centrosome duplication in human cells. *Dev Cell* 3: 339–350

Chivukula RR, Montoro DT, Leung HM, Yang J, Shamseldin HE, Taylor MS, Dougherty GW, Zariwala MA, Carson J, Daniels MLA *et al* (2020) A human ciliopathy reveals essential functions for NEK10 in airway mucociliary clearance. *Nat Med* 26: 244–251

Dobbelaere J, Schmidt Cernohorska M, Huranova M, Slade D, Dammermann A (2020) Cep97 is required for centriole structural integrity and cilia formation in *Drosophila*. *Curr Biol* 30: 3045–3056.e3047

Gartenmann L, Wainman A, Qurashi M, Kaufmann R, Schubert S, Raff JW, Dobbie IM (2017) A combined 3D-SIM/SMLM approach allows centriole proteins to be localized with a precision of ∼4-5 nm. *Curr Biol* 27: R1054–r1055

Goetz SC, Liem Jr KF, Anderson KV (2012) The spinocerebellar ataxia-associated gene Tau tubulin kinase 2 controls the initiation of ciliogenesis. *Cell* 151: 847–858

Huang N, Zhang D, Li F, Chai P, Wang S, Teng J, Chen J (2018) M-phase phosphoprotein 9 regulates ciliogenesis by modulating CP110-CEP97 complex localization at the mother centriole. *Nat Commun* 9: 4511

Klena NT, Gibbs BC, Lo CW (2017) Cilia and ciliopathies in congenital heart disease. *Cold Spring Harb Perspect Biol* 9: a028266

Kleylein-Sohn J, Westendorf J, Le Clech M, Habedanck R, Stierhof YD, Nigg EA (2007) Plk4-induced centriole biogenesis in human cells. *Dev Cell* 13: 190–202

Knödler A, Feng S, Zhang J, Zhang X, Das A, Peränen J, Guo W (2010) Coordination of Rab8 and Rab11 in primary ciliogenesis. *Proc Natl Acad Sci USA* 107: 6346–6351

Kobayashi T, Tsang WY, Li J, Lane W, Dynlacht BD (2011) Centriolar kinesin Kif24 interacts with CP110 to remodel microtubules and regulate ciliogenesis. *Cell* 145: 914–925

Kong D, Sahabandu N, Sullenberger C, Vásquez-Limeta A, Luvsanjav D, Lukasik K, Loncarek J (2020) Prolonged mitosis results in structurally aberrant and over-elongated centrioles. *J Cell Biol* 219: jcb.20191001906192020c

L'Hernault SW, Rosenbaum JL (1985) Chlamydomonas alpha-tubulin is posttranslationally modified by acetylation on the epsilon-amino group of a lysine. *Biochemistry* 24: 473–478

Liu Z, Nguyen QPH, Nanjundappa R, Delgehyr N, Megherbi A, Doherty R, Thompson J, Jackson C, Albulescu A, Heng YM *et al* (2020) Super-resolution microscopy and FIB-SEM imaging reveal parental centriole-derived, hybrid cilium in mammalian multiciliated cells. *Dev Cell* 55: 224–236.e226

Loukil A, Tormanen K, Sutterlin C (2017) The daughter centriole controls ciliogenesis by regulating Neurl-4 localization at the centrosome. *J Cell Biol* 216: 1287–1300

Meitinger F, Ohta M, Lee K-Y, Watanabe S, Davis RL, Anzola JV, Kabeche R, Jenkins DA, Shiau AK, Desai A *et al* (2020) TRIM37 controls cancer-specific vulnerability to PLK4 inhibition. *Nature* 585: 440–446

Mönnich M, Borgeskov L, Breslin L, Jakobsen L, Rogowski M, Doganli C, Schröder JM, Mogensen JB, Blinkenkjær L, Harder LM *et al* (2018) CEP128 localizes to the subdistal appendages of the mother centriole and regulates TGF-β/BMP signaling at the primary cilium. *Cell Rep* 22: 2584–2592

Mookherjee S, Chen HY, Isgrig K, Yu W, Hiriyanna S, Levron R, Li T, Colosi P, Chien W, Swaroop A *et al* (2018) A CEP290 C-terminal domain complements the mutant CEP290 of Rd16 mice in trans and rescues retinal degeneration. *Cell Rep* 25: 611–623.e616

Nachury MV, Mick DU (2019) Establishing and regulating the composition of cilia for signal transduction. *Nat Rev Mol Cell Biol* 20: 389–405

Nigg EA, Holland AJ (2018) Once and only once: mechanisms of centriole duplication and their deregulation in disease. *Nat Rev Mol Cell Biol* 19: 297–312

Pala R, Jamal M, Alshammari Q, Nauli SM (2018) The roles of primary cilia in cardiovascular diseases. *Cells* 7: 233

Paz J, Lüders J (2018) Microtubule-organizing centers: towards a minimal parts list. *Trends Cell Biol* 28: 176–187

Pellicciotta N, Hamilton E, Kotar J, Faucourt M, Delgehyr N, Spassky N, Cicuta P (2020) Entrainment of mammalian motile cilia in the brain with hydrodynamic forces. *Proc Natl Acad Sci USA* 117: 8315–8325

Reiter JF, Leroux MR (2017) Genes and molecular pathways underpinning ciliopathies. *Nat Rev Mol Cell Biol* 18: 533–547

Ridder III WH, Nusinowitz S (2006) The visual evoked potential in the mouse–origins and response characteristics. *Vision Res* 46: 902–913

Sánchez I, Dynlacht BD (2016) Cilium assembly and disassembly. *Nat Cell Biol* 18: 711–717

Schmidt KN, Kuhns S, Neuner A, Hub B, Zentgraf H, Pereira G (2012) Cep164 mediates vesicular docking to the mother centriole during early steps of ciliogenesis. *J Cell Biol* 199: 1083–1101

Schmidt TI, Kleylein-Sohn J, Westendorf J, Le Clech M, Lavoie SB, Stierhof YD, Nigg EA (2009) Control of centriole length by CPAP and CP110. *Curr Biol* 19: 1005–1011

Shoda T, Yamazoe K, Tanaka Y, Asano Y, Inoue YH (2021) Orbit/CLASP determines centriole length by antagonising Klp10A in *Drosophila* spermatocytes. *J Cell Sci* 134: jcs251231

Sigg MA, Menchen T, Lee C, Johnson J, Jungnickel MK, Choksi SP, Garcia G, Busengdal H, Dougherty GW, Pennekamp P *et al* (2017) Evolutionary proteomics uncovers ancient associations of cilia with signaling pathways. *Dev Cell* 43: 744–762.e711

Song R, Walentek P, Sponer N, Klimke A, Lee JS, Dixon G, Harland R, Wan Y, Lishko P, Lize M *et al* (2014) miR-34/449 miRNAs are required for motile ciliogenesis by repressing cp110. *Nature* 510: 115–120

Spassky N, Meunier A (2017) The development and functions of multiciliated epithelia. *Nat Rev Mol Cell Biol* 18: 423–436

Spektor A, Tsang WY, Khoo D, Dynlacht BD (2007) Cep97 and CP110 suppress a cilia assembly program. *Cell* 130: 678–690

Tsang WY, Dynlacht BD (2013) CP110 and its network of partners coordinately regulate cilia assembly. *Cilia* 2: 9

Tu H-Q, Qin X-H, Liu Z-B, Song Z-Q, Hu H-B, Zhang Y-C, Chang Y, Wu M, Huang Y, Bai Y-F *et al* (2018) Microtubule asters anchored by FSD1 control axoneme assembly and ciliogenesis. *Nat Commun* 9: 5277

Vertii A, Hung HF, Hehnly H, Doxsey S (2016) Human basal body basics. *Cilia* 5: 13

Vieillard J, Paschaki M, Duteyrat JL, Augière C, Cortier E, Lapart JA, Thomas J, Durand B (2016) Transition zone assembly and its contribution to axoneme formation in *Drosophila* male germ cells. *J Cell Biol* 214: 875–889

Walentek P, Quigley IK, Sun DI, Sajjan UK, Kintner C, Harland RM (2016) Ciliary transcription factors and miRNAs precisely regulate Cp110 levels required for ciliary adhesions and ciliogenesis. *Elife* 5: e17557

Walia V, Cuenca A, Vetter M, Insinna C, Perera S, Lu Q, Ritt DA, Semler E, Specht S, Stauffer J *et al* (2019) Akt regulates a Rab11-effector switch required for ciliogenesis. *Dev Cell* 50: 229–246.e227

Wallmeier J, Nielsen KG, Kuehni CE, Lucas JS, Leigh MW, Zariwala MA, Omran H (2020) Motile ciliopathies. *Nat Rev Dis Primers* 6: 77

Willaredt MA, Gorgas K, Gardner HA, Tucker KL (2012) Multiple essential roles for primary cilia in heart development. *Cilia* 1: 23

Williams CL, Li C, Kida K, Inglis PN, Mohan S, Semenec L, Bialas NJ, Stupay RM, Chen N, Blacque OE *et al* (2011) MKS and NPHP modules cooperate to establish basal body/transition zone membrane associations and ciliary gate function during ciliogenesis. *J Cell Biol* 192: 1023–1041

Xu J (2005) Preparation, culture, and immortalization of mouse embryonic fibroblasts. *Curr Protoc Mol Biol* Chapter 28: Unit 28 21

Yang Y, Ran J, Liu M, Li D, Li Y, Shi X, Meng D, Pan J, Ou G, Aneja R *et al* (2014) CYLD mediates ciliogenesis in multiple organs by deubiquitinating Cep70 and inactivating HDAC6. *Cell Res* 24: 1342–1353

Yu F, Li TE, Sui Y, Chen Q, Yang S, Yang J, Hong R, Li D, Yan X, Zhao W *et al* (2020) O-GlcNAc transferase regulates centriole behavior and intraflagellar transport to promote ciliogenesis. *Protein Cell* 11: 852–857